

## Electronic effects on melting: Comparison of aluminum cluster anions and cations

Anne K. Starace,<sup>1</sup> Colleen M. Neal,<sup>1</sup> Baopeng Cao,<sup>1</sup> Martin F. Jarrold,<sup>1,a)</sup>  
 Andrés Aguado,<sup>2,b)</sup> and José M. López<sup>2</sup>

<sup>1</sup>Department of Chemistry, Indiana University, 800 East Kirkwood Ave., Bloomington, Indiana 47405, USA

<sup>2</sup>Departamento de Física Teórica, Universidad de Valladolid, Valladolid 47011, Spain

(Received 8 March 2009; accepted 2 June 2009; published online 23 July 2009;  
 corrected 24 July 2009)

Heat capacities have been measured as a function of temperature for aluminum cluster anions with 35–70 atoms. Melting temperatures and latent heats are determined from peaks in the heat capacities; cohesive energies are obtained for solid clusters from the latent heats and dissociation energies determined for liquid clusters. The melting temperatures, latent heats, and cohesive energies for the aluminum cluster anions are compared to previous measurements for the corresponding cations. Density functional theory calculations have been performed to identify the global minimum energy geometries for the cluster anions. The lowest energy geometries fall into four main families: distorted decahedral fragments, fcc fragments, fcc fragments with stacking faults, and “disordered” roughly spherical structures. The comparison of the cohesive energies for the lowest energy geometries with the measured values allows us to interpret the size variation in the latent heats. Both geometric and electronic shell closings contribute to the variations in the cohesive energies (and latent heats), but structural changes appear to be mainly responsible for the large variations in the melting temperatures with cluster size. The significant charge dependence of the latent heats found for some cluster sizes indicates that the electronic structure can change substantially when the cluster melts. © 2009 American Institute of Physics.

[DOI: 10.1063/1.3157263]

### I. INTRODUCTION

It is now well established that metal clusters with 10–10<sup>3</sup> atoms can display transitions between solidlike and liquidlike states. The transitions have first order characteristics and have been observed in experiments by means of a peak in the heat capacity due to the latent heat. Most of the experimental studies performed so far have focused on sodium<sup>1–11</sup> and aluminum clusters.<sup>12–18</sup>

Sodium, in particular, has played a special role in the development of our understanding of the properties of metal clusters.<sup>19,20</sup> The “magic numbers” observed for sodium clusters led to the development of the electronic shell model,<sup>21</sup> and several properties of sodium clusters (for example, ionization energies, electron affinities, and the dissociation energies of smaller clusters) can be rationalized using free electron models where discontinuities occur at electronic shell closings. For example, the sharp drops in the dissociation energies for sodium cluster cations Na<sub>n</sub><sup>+</sup> with  $n=9$  and 21 are associated with the opening of new electronic shells.<sup>22</sup> The electronic shell models ignore the geometric structures, except for the possibility of ellipsoidal distortions between spherical shell closings.<sup>23</sup>

The experimental studies of cluster melting have revealed significant size dependent fluctuations in the melting temperatures. In the case of sodium clusters, the maxima and

minima are not correlated with electronic shell closings. In retrospect this is perhaps not surprising. The liquid and solid clusters have the same number of electrons and so melting might not cause a significant change in the electronic shell structure. For sodium clusters, the variations in the latent heats and melting temperatures seem to be correlated, and so maxima in the latent heats are also not correlated with the electronic shell closings. On the contrary, it appears that the features observed in the melting temperatures and latent heats for sodium clusters can be explained by geometric shell closings for icosahedral packing.<sup>8,24,25</sup>

We recently showed that the latent heats for melting are correlated with the solid cluster cohesive energies.<sup>18</sup> Maxima in the latent heats occur for clusters that are particularly strongly bound. In the case of aluminum clusters, we found that enhanced stability results from a combination of geometric and electronic shell effects. For some clusters (e.g., Al<sub>37</sub><sup>+</sup>) an electronic shell closing is responsible for the enhanced cohesive energy and large latent heat, while for others (e.g., Al<sub>44</sub><sup>+</sup>) a geometric shell closing is responsible. Thus unlike sodium, where the melting properties can be explained by a structural model, for aluminum, the electronic structure and geometric structure both contribute.

However, one should keep in mind an important difference between the experiments on sodium and aluminum: For aluminum, clusters as small as Al<sub>28</sub><sup>+</sup> show a melting transition, and melting properties have been systematically measured down to that size. For sodium, such small clusters melt

<sup>a)</sup>Electronic mail: mfj@indiana.edu.

<sup>b)</sup>Electronic mail: aguado@metodos.fam.cie.uva.es.

gradually<sup>26</sup> without an appreciable latent heat, and so the detailed (atom by atom) size evolution of melting properties has only been measured for much larger clusters with 100–360 atoms. Then, as suggested in one of our previous papers,<sup>18</sup> the differences between the results for sodium and aluminum clusters may not be as large as they initially appear. The cohesive energies for solid sodium clusters with 135–154 atoms were calculated and showed a significant drop at  $n=148$  after the icosahedral shell closing and only a tiny drop at  $n=139$  after the electronic shell closing. These variations in the cohesive energies correlate with the fluctuations in the latent heats for sodium clusters in this size range, where only the geometric shell closing causes a significant change in the latent heat.<sup>8</sup> For much smaller sodium clusters, melting is expected to be affected by electron shell closings as well, as suggested by some recent simulations.<sup>27</sup> Similarly, the melting of much larger aluminum clusters is expected to be dominated by structural effects. The only difference between sodium and aluminum clusters would then be the critical size where electronic effects on the solid cohesive energies (and on latent heats) become negligible compared to structural effects.

In this manuscript we further investigate the influence of electronic structure on melting by comparing the results for aluminum cluster anions with previous measurements for the corresponding cations. The anions and cations have the same number of atoms, but the anions have two extra electrons. We report the measurements of the heat capacities as a function of temperature for  $\text{Al}_n^-$  with  $n=35-70$ . From the position and size of the peaks in the heat capacities we determine the melting temperatures and the latent heats for melting.

Dissociation energies for the cluster anions have been obtained by analyzing the measured dissociation thresholds using a statistical model. For clusters that melt before they dissociate, this approach leads to the dissociation energy for the liquid cluster.<sup>18</sup> Dissociation energies (and cohesive energies) for the solid clusters are obtained from the measured (liquid) dissociation energies and the latent heats.

In addition to these experimental studies, we have performed calculations to identify the global minimum energy geometries for aluminum cluster anions with 35–70 atoms. The calculations were performed at the Kohn–Sham density functional theory (DFT) level. The cohesive energies for the lowest energy geometries found in the calculations for each cluster size are compared to the cohesive energies obtained from the experiments. This allows us to interpret the size variation in the latent heats of melting. We have also performed similar calculations for neutral aluminum clusters with 35–70 atoms. Although the melting properties of neutral clusters cannot be investigated in the experiments at present, these calculations help interpret the differences between the latent heats of the anions and cations.

## II. EXPERIMENTAL METHODS

The experimental apparatus and methods used here are described in detail elsewhere.<sup>14,28</sup> Briefly, aluminum cluster ions are generated by laser vaporization of a liquid metal target in a continuous flow of helium buffer gas. The clusters

are carried out of the source region and into a 10 cm long temperature variable extension where they reach thermal equilibrium and their temperature is set. The clusters exit the extension and they are focused into a quadrupole mass spectrometer set to transmit a particular cluster size. The size-selected clusters are then focused into a collision cell containing 1.0 torr of helium. As the clusters enter the collision cell they undergo many collisions with the helium collision gas, each one converting a small fraction of the cluster's translational energy into internal energy and translational energy of the helium collision partner. If the cluster's initial translational energy is large enough, some of them are heated to the point where they dissociate. They fragment by the sequential loss of aluminum atoms. The products and undissociated cluster ions are drawn across the collision cell by a weak electric field and some exit through a small aperture. The ions that exit are focused into a second quadrupole mass spectrometer where they are analyzed and then detected with a collision dynode and microchannel plates. The fraction of the clusters that dissociate is determined from the mass spectrum.

Measurements are typically performed at six translational energies and a linear regression is used to determine the translational energy required to dissociate 50% of the clusters (TE50%D). TE50%D is then measured as a function of the temperature of the extension. As this temperature is raised the internal energy of the clusters increases and TE50%D decreases. When the cluster melts, the latent heat causes TE50%D to decrease more sharply. The derivative of TE50%D with respect to temperature is proportional to the heat capacity.

## III. EXPERIMENTAL RESULTS

Figure 1 shows a plot of the heat capacities recorded as a function of temperature for  $\text{Al}_{35}^-$  to  $\text{Al}_{70}^-$ . The results are plotted in terms of the classical value  $3Nk_B$  where  $3N=3n-6+3/2$ ,  $n$  is the number of atoms in the cluster, and  $k_B$  is the Boltzmann constant. The points are the experimental results (an average of at least three independent measurements), the solid line going through the points is a spline fit, and the thin dashed line is the heat capacity derived from a modified Debye model.<sup>29</sup>

Significant peaks in the heat capacities indicate melting transitions. For example, for  $\text{Al}_{35}^-$  there is a substantial and relatively broad peak at slightly below 900 K. The peak becomes smaller and shifts to around 600 K for  $\text{Al}_{41}^-$ . For  $\text{Al}_{43}^-$  the peak has a substantial shoulder at higher temperature. The melting transition for  $\text{Al}_{46}^-$  is broader and is shifted to  $\sim 750$  K. The heat capacities for  $\text{Al}_{47}^-$  do not show an obvious melting transition. However, the transition reappears for  $\text{Al}_{48}^-$  at  $\sim 600$  K and fluctuates around this value until  $\text{Al}_{64}^-$ . Some clusters ( $\text{Al}_{52}^-$  and  $\text{Al}_{55}^-$ ) have broad asymmetric heat capacity peaks while others (for example,  $\text{Al}_{56}^-$  and  $\text{Al}_{61}^-$ ) show dips in the heat capacities at a lower temperature than the peak due to the melting transition. From  $\text{Al}_{64}^-$  to  $\text{Al}_{67}^-$  the peak in the heat capacity jumps up to around 900 K, although for  $\text{Al}_{64}^-$  and  $\text{Al}_{67}^-$  the peak is small and broad and not very prominent. From  $\text{Al}_{68}^-$  to  $\text{Al}_{70}^-$  the peak is below 600 K.

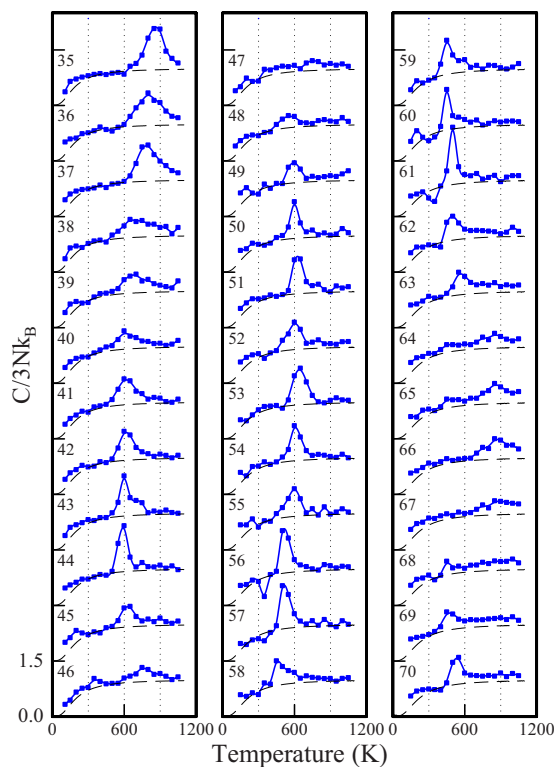


FIG. 1. Heat capacities recorded as a function of temperature for aluminum cluster anions with 35–70 atoms. The heat capacities are plotted relative to the classical value  $3Nk_B$ , where  $3N=3n-6+3/2$  and  $k_B$  is the Boltzmann constant. The filled (blue) squares are the experimental measurements. The solid (blue) lines running through the points are spline fits. The thin black dashed line is the heat capacity derived from a modified Debye model (Ref. 29).

Figure 2 shows a comparison of the heat capacities for selected  $Al_n^-$  with those for the corresponding cations. The comparison shown in this figure is representative of the behavior found for other cluster sizes. In some cases,  $n=42$ , 52, and 54, for example, addition of the two extra electrons causes only minor differences to the heat capacities. For other cluster sizes there are substantial differences in the melting temperature (e.g.,  $n=37$  and 44), size of the peak (e.g.,  $n=39$  and 61), and the shape of the peak (e.g.,  $n=43$  and 51).

In our previous studies of the heat capacities of aluminum cluster cations we fit the experimental results with two and three state models.<sup>13</sup> The same approach has been implemented here. We assume that melting and freezing occur in the dynamic coexistence regime where the transitions are between fully liquid and fully solid clusters.<sup>30–33</sup> In this limit, the liquid and solid are in equilibrium, and the equilibrium constant is

$$K(T) = \exp\left[-\frac{\Delta H_m}{R}\left(\frac{1}{T} - \frac{1}{T_m}\right)\right], \quad (1)$$

where  $\Delta H_m$  is the latent heat,  $T_m$  is the melting temperature, and  $R$  is the gas constant. The contribution of the latent heat to the heat capacity is

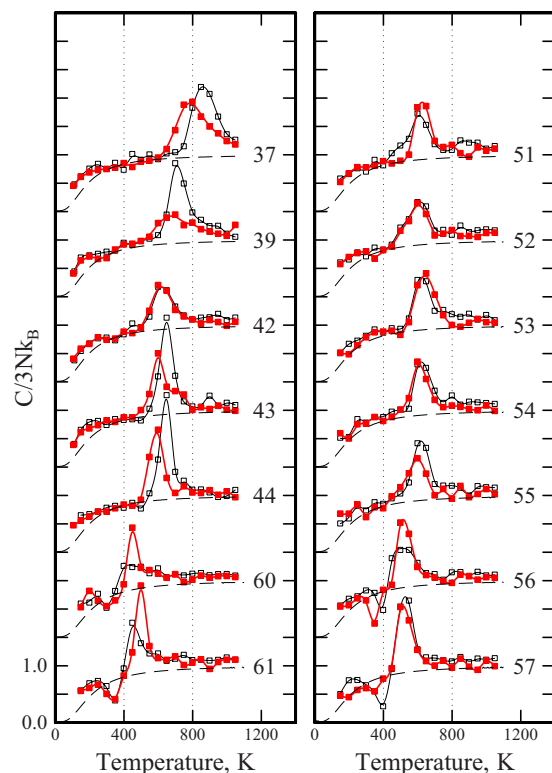


FIG. 2. Comparison of the heat capacities recorded for aluminum cluster anions and cations with 37, 39, 42–44, 60, 61, and 51–57. The heat capacities are plotted relative to the classical value  $3Nk_B$ , where  $3N=3n-6+3/2$  and  $k_B$  is the Boltzmann constant. The filled (red) points are for the anions and the unfilled (black) points are for the cations. The solid lines running through the points are spline fits. The thin black dashed line is the heat capacity derived from a modified Debye model (Ref. 29).

$$C(T) = \frac{dE_{\text{int}}}{dT} = \frac{\Delta(-f_S(T)\Delta H_m)}{\Delta T}, \quad (2)$$

where  $f_S(T)$  is the fraction of solid clusters present at temperature  $T$ . We add this to the component of the heat capacity due to the internal energy of the solid and liquid clusters. For both we use the heat capacity derived from the modified Debye model multiplied by a scale factor. The simulation is fit to the measured heat capacities using a least-squares procedure with four adjustable parameters:  $\Delta H_m$ ,  $T_m$ ,  $S_S$ , and  $S_L$ , where  $S_S$  and  $S_L$  are scale factors.

Examples of the fits are shown in Fig. 3. The experimental results are represented by the filled black squares and the fits are represented by the unfilled (blue) circles and the solid (blue) lines. The results for  $Al_{44}^-$  and  $Al_{66}^-$  were obtained with the two state model, which provides a good fit to the experimental results (except at low temperature). The lines at the bottom of each plot show the relative abundances (using the scale on the right hand axes) of the solid (light green) and liquid (dark green), respectively.

For the other clusters in Fig. 3 the fit obtained with the two state model was found to be inadequate and a three state model incorporating a partially melted intermediate ( $S \rightleftharpoons I \rightleftharpoons L$ ) was used. For  $Al_{60}^-$  and  $Al_{61}^-$  there is a shoulder on the high temperature side of the main peak in the heat capacity. Interestingly,  $Al_{61}^+$  also has a high temperature shoulder on its heat capacity peak.<sup>13</sup> The lines at the bottom

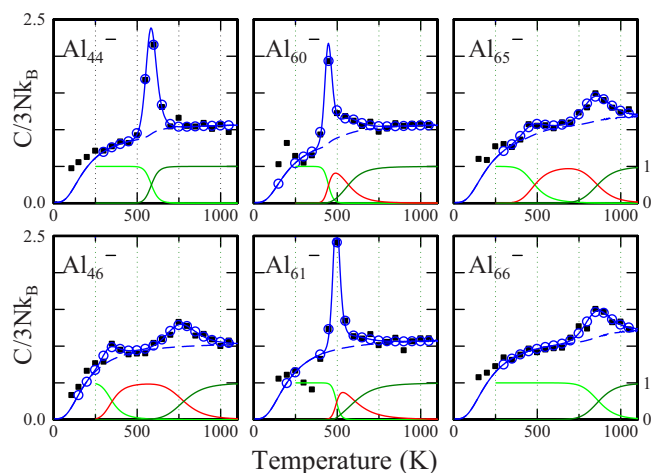


FIG. 3. Examples of fits of the two and three state models to the heat capacities for aluminum cluster anions. The filled black points are the experimental results. The unfilled (blue) circles are simulations with the value of  $\Delta T$  used to determine the heat capacities set to 50 K (the same value as used in the experiments). The solid (blue) line shows heat capacities calculated using  $\Delta T=5$  K. The dashed (blue) line shows the calculated heat capacity without the contribution from the latent heat. The results for  $n=44$  and 66 are for the two state model. The lines at the bottom of these plots show the calculated relative abundances (using the scale on the right hand axes) of the solid (dark green) and liquid (light green) clusters as a function of temperature. The results for  $n=46, 60, 61,$  and 65 were obtained with the three state model. The lines at the bottom of these plots show the calculated relative abundances of the solid (dark green), intermediate (red), and liquid (light green) clusters as a function of temperature.

of each plot in Fig. 3 show the abundances of the solid (light green), intermediate (red), and liquid (dark green), respectively. For  $\text{Al}_{46}^-$  and  $\text{Al}_{65}^-$  there appear to be two small peaks in the heat capacities that are separated by more than 450 K.

Figure 4 shows the melting temperatures derived from the fits. The unfilled black circles are the results for the cations (from previous work<sup>13</sup>) and the filled (red) points are for the anions. Where there are two well resolved peaks in the heat capacities (i.e., for  $\text{Al}_{46}^-$  and  $\text{Al}_{65}^-$  in Fig. 3) we show values for both transition temperatures. When the peaks are not resolved (i.e., for  $\text{Al}_{60}^-$  and  $\text{Al}_{61}^-$  in Fig. 3) we only show the transition temperature associated with the dominant feature. We do not show peaks with transition temperatures less than 300 K. For example, there is a broad peak for  $\text{Al}_{45}^-$  centered around 200 K, which is not included in the plot.

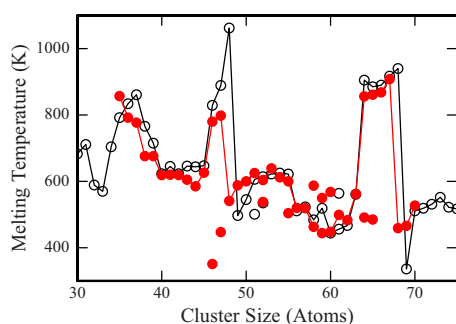


FIG. 4. Plot of the melting temperatures determined for aluminum clusters. The filled (red) points show results for the anions and the unfilled points show results for the cations (the data for the cations are taken from Ref. 13). Where there are two well-resolved peaks in the heat capacities (i.e., for  $\text{Al}_{46}^-$  and  $\text{Al}_{65}^-$ ) we show values for both transitions.

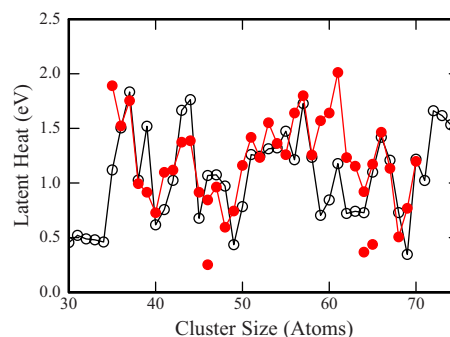


FIG. 5. Plot of the latent heats determined from the heat capacities for aluminum clusters. The filled (red) points show results for the anions and the unfilled points show results for the cations (the data for the cations are taken from Ref. 13). Where there are two well-resolved peaks in the heat capacities (i.e., for  $\text{Al}_{46}^-$  and  $\text{Al}_{65}^-$ ) we show values for both transitions.

Several other clusters have features in their low temperature ( $<300$  K) heat capacities. In some cases these features may not be real, but the low temperature peak for  $\text{Al}_{45}^-$  is definitely reproducible.

The melting temperatures for the anions and cations show the same general trends with peaks at around  $n=36, 46,$  and 65. Note that the features in the melting temperatures of the anions appear to be shifted to slightly smaller cluster size than for the cations.

Figure 5 shows the latent heats plotted against the cluster size for anions [filled (red) circles] and cations (unfilled [black circles]) from previous work.<sup>13</sup> For  $\text{Al}_{46}^-$ ,  $\text{Al}_{64}^-$ , and  $\text{Al}_{65}^-$ , where there are clearly two well-separated features in the heat capacities we show latent heats for both obtained from the three state model. For cases where the two state model provides an excellent fit to the experimental data we show the latent heat derived from the two state model. For intermediate cases, we manually interpolated between the values derived from the two state and three state models, usually by starting with the two state fit and adding a contribution to account for a missing shoulder.

We use the change in the TE50%D values with temperature to determine the heat capacities. However, the TE50%D values themselves can also be analyzed using a statistical model to determine the dissociation energy of the clusters. To do this we use the same model recently employed to analyze the dissociation thresholds of the aluminum cluster cations. We briefly describe the model here; a more detailed description can be found elsewhere.<sup>18</sup> The fraction of the clusters that dissociate is given by

$$f = \frac{\int_0^\infty dE_V \rho_V(E_V) e^{-E_V/k_B T} (1 - e^{-k(E,D)t})}{\int_0^\infty dE_V \rho_V(E_V) e^{-E_V/k_B T}}, \quad (3)$$

where  $E_V$  is the initial vibrational energy of the cluster,  $T$  is the temperature of the source extension,  $t$  is the time that the clusters remain hot, and  $\rho_V$  is the vibrational density of states.  $k(E,D)$  is the rate constant for unimolecular dissociation of a cluster with dissociation energy  $D$  and total internal energy  $E$ . We use the quantum Rice-Ramsperger-Kassel (RRK) model<sup>34</sup> for the reaction rate constant

$$k(E, D) = g \nu \frac{p! (p - q + s - 1)!}{(p + s - 1)! (p - q)!}, \quad (4)$$

with  $p = E/h\nu$ ,  $q = D/h\nu$ , and  $s = 3n - 6$ .  $\nu$  is the characteristic vibrational frequency of the cluster,  $n$  is the number of atoms in the cluster, and  $g$  is the reaction path degeneracy (the number of equivalent ways the reaction can occur).

The clusters melt before they dissociate, and so dissociation occurs from the liquid state. Thus the dissociation energy determined using the approach described above is the dissociation energy of the liquid cluster  $D_L$ . The total internal energy of the liquid cluster  $E$  is<sup>18</sup>

$$E = E_V + E_C - L^0(n), \quad (5)$$

where  $E_V$  is the initial vibrational energy in the solid cluster,  $E_C$  is the internal energy added by the collisions, and  $L^0(n)$  is the energy difference between the solid and liquid clusters at 0 K, which we approximate by the measured latent heat.

The dissociation of a liquid cluster could yield an  $(n-1)$  atom product that is liquid or, if evaporation and freezing occur simultaneously, solid. For the cluster sizes studied here, evaporation of a single atom does not cool the cluster enough for it to be able to freeze, and so the  $(n-1)$  atom product must be liquid.<sup>18</sup> In this case, the relationship between the dissociation energy of the solid cluster  $D_S$  and the dissociation energy of the liquid  $D_L$  is

$$D_S = D_L + L^0(n) - L^0(n-1), \quad (6)$$

where  $L^0(n)$  is the energy difference between the liquid and solid  $n$  atom cluster at 0 K and  $L^0(n-1)$  is the energy difference between the liquid and solid  $(n-1)$  atom product at 0 K.  $L^0(n)$  and  $L^0(n-1)$  are both approximated by the measured latent heats.

The cluster cohesive energies are given by

$$C_S(n) = \frac{\sum D_S(n)}{n} = \frac{\sum [D_L(n) + L^0(n) - L^0(n-1)]}{n} \approx \frac{L(n) + \sum D_L(n)}{n}. \quad (7)$$

Since the dissociation energies of the liquid clusters change smoothly with  $n$ ,<sup>18</sup> the variation in the cohesive energies of the solid clusters will track the variations in the latent heats. The cohesive energies are shown in Fig. 6 for both the anions and the cations as the filled black points. The unfilled (red) circles in Fig. 6 show cohesive energies derived from the lowest energy structures found in DFT calculations (see below). In the experimental work reported here, dissociation energies were determined for aluminum cluster anions with 35–70 atoms, and so in order to convert the measured dissociation energies into cohesive energies it is necessary to assume a value for the cohesive energy of  $\text{Al}_{34}^-$  (because an experimental value is not available). For the results shown in Fig. 6 we chose a value that led to the best overlap with the calculated cohesive energies. A similar approach was adopted for the cations, where the cohesive energy of  $\text{Al}_{24}^+$  was adjusted to provide the best fit to the calculated cohesive energies. In what follows, we focus mainly on whether or not

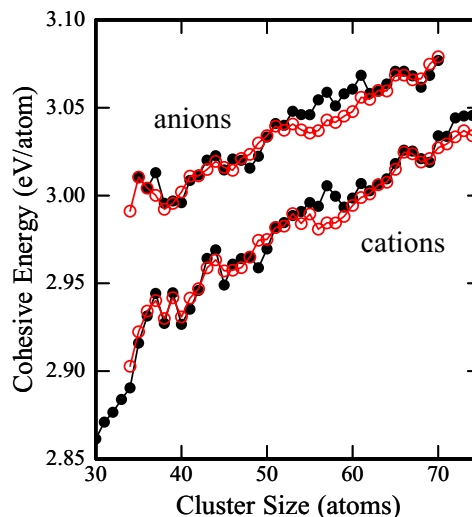


FIG. 6. Cohesive energies for aluminum cluster anions compared to corresponding results for the cations (Ref. 18). The filled black points show results derived from experimental measurements. The unfilled (red) points show results obtained from calculations using DFT.

the calculated cohesive energies are able to match the size dependent variations in the measured values.

The comparison of the cohesive energies of the aluminum cluster anions and cations (filled black points in Fig. 6) reveals both similarities and differences. For the cations, there are local maxima in the cohesive energies at 37, 39, 42–43, 57, 61, and 66–67 atoms. For the anions, there is a new maximum at 35 atoms, the maximum at 39 atoms is absent, and the maximum at 42 and 43 atoms is much less pronounced. The maxima at 57, 61, and 66 and 67 atoms also seem to be less pronounced for the anions than for the cations.

#### IV. COMPUTATIONAL METHODS

Calculations were performed at the Kohn–Sham DFT level,<sup>35</sup> employing the SIESTA code.<sup>36</sup> The spin-polarized generalized gradient expression of Perdew *et al.*<sup>37</sup> was employed to approximate the exchange–correlation energy. All other computational details such as the pseudopotential, basis set, and the size of the fast-Fourier-transform mesh are exactly the same as in our previous work.<sup>17,18,38,39</sup> The accuracy of the calculations was assessed in the previous work by comparisons with the results of other first-principles techniques. An independent assessment has been provided by Henry *et al.*<sup>40</sup> The optimization strategy employed to obtain the global minimum structures of anionic and neutral aluminum clusters with 35–70 atoms is also exactly the same as that employed in previous work, so we refer the reader to Ref. 39 for details.

#### V. COMPUTATIONAL RESULTS

A representative selection of the structures of the cluster anions is shown in Fig. 7, and the atomic coordinates for all putative global minima will be made available through the internet.<sup>41</sup> The structures can be grouped into the same four types which were found for cations,<sup>18</sup> namely, distorted decahedral fragment (ddf), fragments of a face-centered-cubic

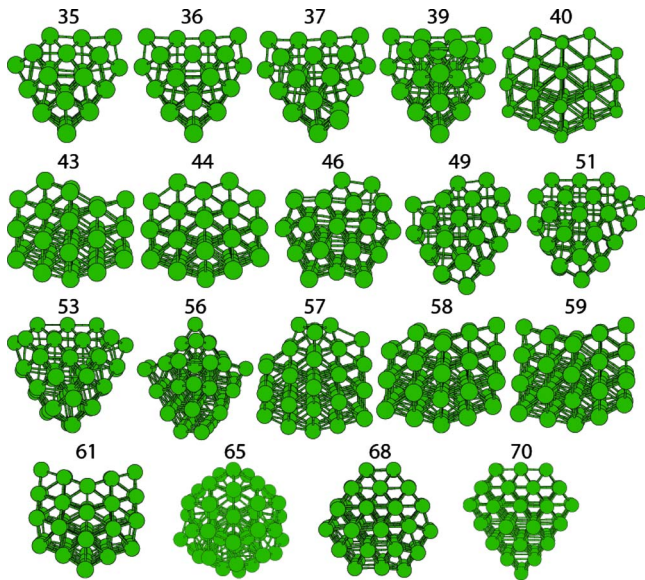


FIG. 7. A selection of cluster anion structures. The number of atoms in the cluster is shown on top of each structure. The structural families identified here are the same as for the cluster cations (Ref. 18): ddf around 36 and 53 atoms, disordered isomers around 46 and 66 atoms, and fcc-like fragments (with or without sf) for the rest of the sizes. The disordered isomers for  $n=45$  and 46 (which are not shown in the figure) are nearly degenerate with the ordered global minima.

(fcc) lattice, fcc fragments with stacking fault (sf), and other “disordered” rounded structures (dis) characterized by a crowded cluster core and a wider distribution of bond lengths. Isomers of these structural families become the global minima over different size ranges.

The global structural size evolution is similar for both cations and anions. In the lower size range of around 35–38 atoms, the global minima belong to the ddf family. The sf isomers then become more stable up to 44 atoms. Close to the spherical electronic shell closing at 138 electrons (46 atoms) disordered isomers appear, which are nearly degenerate with the sf isomers. For  $\text{Al}_{46}^+$  the disordered isomer is the global minimum while for  $\text{Al}_{46}^-$  the global minimum is an ordered sf isomer, but the energy differences between both isomers are very small, less than 2 meV/atom. The ddf structures dominate again at around 50–55 atoms and fcc or sf structures for 56–63 atoms. When the number of electrons approaches 198 (66 atoms), another spherical electronic shell closing, the disordered rounded structures become the global minima again. The fcc or sf structures are recovered for 69–70 atoms.

A detailed comparison of cation and anion structures shows that there are many subtle differences. The global minimum isomer is the same for cation and anion for only 16 sizes (out of a total of 36 considered here). For the rest of the sizes (more than 50% of the total), the cluster charge modifies the minimum energy structure. For twelve sizes the differences are not very important: The cation and anion belong to the same structural family but the distribution of vacancies or adatoms at the cluster surface is not exactly the same. For the remaining eight sizes, the cation and anion belong to different structural families and so the differences are sub-

stantial. This always occurs close to the critical transition sizes between the different structural families.

The cohesive energies for the lowest energy geometry found for each cluster size are shown in Fig. 6 as the unfilled (red) circles. The cohesive energies are defined by

$$C_S^-(n) = \frac{-[E(\text{Al}_n^-) - (n-1)E(\text{Al}) - E(\text{Al}^-)]}{n} \quad (8)$$

for the anions and by

$$C_S^+(n) = \frac{-[E(\text{Al}_n^+) - (n-1)E(\text{Al}) - E(\text{Al}^+)]}{n} \quad (9)$$

for cations. The difference between these two equations is

$$C_S^-(n) - C_S^+(n) = \frac{[IE(n) - IE(1)] + [EA(n) - EA(1)]}{n}, \quad (10)$$

where  $IE(n)$  and  $EA(n)$  are the ionization energy and electron affinity of the  $n$ -atom cluster. This difference accounts for the shift between the anion and cation curves in Fig. 6. The two contributions to the cohesive energy difference in the above equation have different signs because the ionization energy of a cluster decreases on average with size  $n$ , while the electron affinity increases. The ionization energy of the Al atom is 5.985 eV, and the electron affinity of the isolated Al atom is just 0.446 eV. Typical values for aluminum clusters in the cluster size range examined here are about 3 eV for the electron affinity and around 5.3 eV for the ionization energy (see below). The electron affinity contribution to  $C_S^-(n) - C_S^+(n)$ , which is positive, dominates. The cohesive energies of anions are larger than those of cations simply because of the very small electron affinity of the isolated Al atom. For much larger clusters (large  $n$ ), the cation and anion cohesive energies converge to the same bulk value.

The comparison of the calculated cohesive energies with the experimental values shown in Fig. 6 is reasonable but not perfect. Enhanced cohesive energies are found for anions with  $n=35, 44, 51, 53, 57, 61, 65$ , and 66, in good agreement with experimental measurements. However, the calculations do not reproduce the maximum at  $n=37$ , and the theoretical cohesive energies for  $n=55-61$  are substantially lower than the experimental values. The underestimation of cohesive energies for clusters with around 57 atoms also occurs for cations, although to a smaller extent. Recently, we compared the calculated electron densities of states to photoelectron spectra measured for aluminum cluster anions.<sup>42</sup> The agreement is very poor precisely for  $n=37$  and 57. This confirms that the calculations have missed the global minimum for these sizes.

The structures of neutral aluminum clusters with 34–70 atoms have also been optimized and will be made available through the internet.<sup>41</sup> The neutral clusters favor the same structural families as found for anions and cations and the same sequence of structural transitions. The neutral clusters can adopt the same structure as the cation or the anion depending on the size. For six sizes (out of the 36 considered here) the neutral structure does not coincide with either of

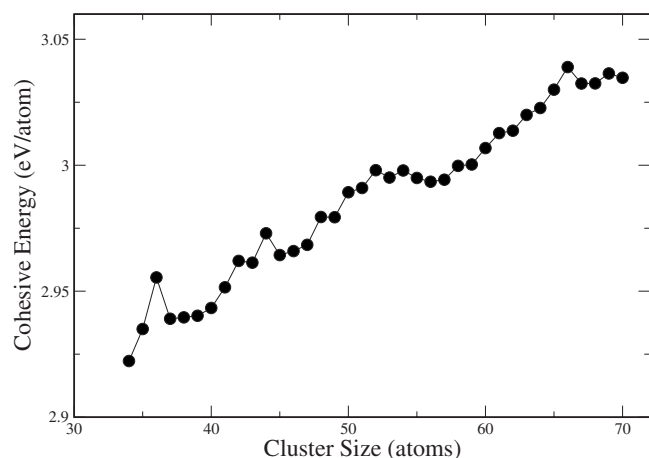


FIG. 8. Cohesive energies of neutral aluminum clusters obtained from the DFT calculations. The corresponding experimental results cannot be obtained with the present experimental method.

the charged structures. The cohesive energies for the lowest energy neutral geometries are shown in Fig. 8. The enhanced stabilities at  $n=36$ , 44, and 66 are more prominent than in the charged clusters. There are also secondary maxima at  $n=52$  and 54 atoms. The comparison of the cohesive energies for the different charge states reveals that a strong magic number appears at  $n=35$  for anions,  $n=36$  for neutrals, and  $n=37$  for cations. There are also enhanced stabilities of secondary importance at  $n=51$  and 53 for anions,  $n=52$  and 54 for neutrals, and  $n=53$  and 55 for cations. The magic numbers at  $n=44$  and 66 are observed for all three charge states, but  $n=43$  and 65 have enhanced stabilities only for the charged clusters.

In our previous work,<sup>18</sup> we showed that the size evolution of the cation stabilities is affected by both structural and electronic contributions. Regarding the structural contribution, we identified two geometric shell closings at  $n=36$  and  $n=44$  atoms. These clusters have perfect (111)-like surface terminations without any vacancies or adatoms on their surface. They also have short and strong bonds and little strain compared to their immediate neighbors. We do not provide a detailed structural analysis here for the neutrals and anions because it is qualitatively the same as for cations (see Fig. 6 of Ref. 18). As expected, when the stability of a cluster has a structural origin, the global minimum is the same for all charge states. This occurs, in particular, for clusters with  $n=36$  and 44 atoms.

In order to analyze the electronic effect on cluster stability, we show in Fig. 9 the adiabatic ionization energies

$$IE(n) = E(\text{Al}_n^+) - E(\text{Al}_n) \quad (11)$$

and electron affinities

$$EA(n) = E(\text{Al}_n) - E(\text{Al}_n^-) \quad (12)$$

of aluminum clusters, where all energies refer to the corresponding global minima. The ionization energies can be directly compared to the photoionization experiments of Schriver *et al.*<sup>43</sup> The theoretical calculations predict large drops in the ionization energy after  $n=36$ , 38, 42, 46, 52, 54, and 66, in good agreement with the experimental measure-

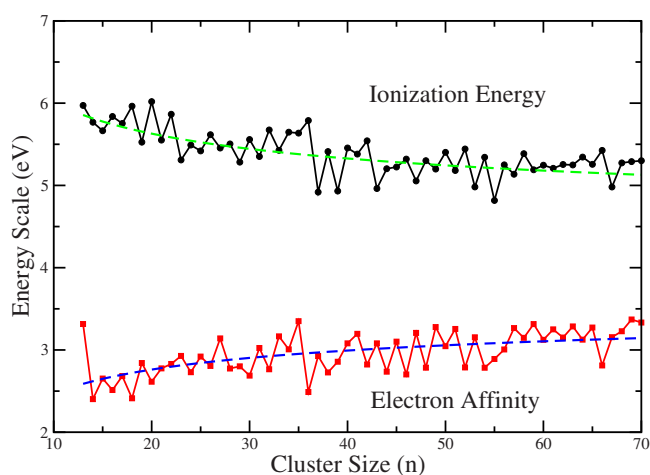


FIG. 9. Calculated adiabatic ionization energies (filled black circles) and electron affinities [filled (red) squares] of neutral aluminum clusters with 13–70 atoms. The dashed lines are fits to a function  $\varphi + An^{-1/3}$ , which represents the smooth size dependence expected from classical charged sphere models. In the case of the ionization energies, the fits give  $\varphi=4.2$  eV, in good agreement with the bulk work function ( $\varphi=4.28$  eV). The results for  $n=13$ –33 are taken from Ref. 39 and are shown here because they are included in the fits.

ments. Those neutral clusters have therefore an enhanced electronic contribution to the cohesive energy.

Because adding one Al atom to a parent cluster introduces three additional electrons, some more analysis is needed to accurately locate the electron shell closings. For  $n=36$ , 46, and 66, we do not have only a large ionization energy drop after adding one more atom, but also a deep minimum in the electron affinity, so  $\text{Al}_{36}$ ,  $\text{Al}_{46}$ , and  $\text{Al}_{66}$  are electron shell closings. The very large electron affinity at  $n=35$  indicates that  $\text{Al}_{35}^-$  is electronically very stable. Similarly, the very low ionization energies at  $n=37$ , 39, 43, 53, and 55 show that the corresponding cations have an enhanced electronic stability.

In summary, the size evolution of the cohesive energies (and therefore of the latent heats) of neutral and anionic clusters results also from the combined action of electronic and structural effects.  $\text{Al}_{35}^-$  is obtained by removing one atom from the geometrical shell closing at  $n=36$ , but it is strongly stabilized by an electron shell closing.  $\text{Al}_{36}$  is both an electronic and structural shell closing, hence its remarkable stability in the neutral series. The structures around  $n=66$  are stabilized by the proximity of an electron shell closing. The high stabilities at  $n=44$  and  $n=61$  are purely structural, so the global minimum is the same for cations, neutrals, and anions. The cluster with 44 atoms is a stronger magic number in the neutral series because it has an even number of electrons, which provides additional stabilization. The cluster with 61 atoms contains some (100)-like, less-densely packed surface facets, and so its stability is not as enhanced as for the 44-atom cluster.

## VI. DISCUSSION

The experimental measurements show that the dissociation energies of liquid aluminum clusters are almost independent of cluster size. Thus the size evolution of the cohesive

energies of the liquid clusters is a smooth function of cluster size, and significant size-dependent fluctuations in the cohesive energies of the solid clusters must result almost entirely from fluctuations in the latent heats. It follows that purely static theoretical calculations, as presented in the preceding section, can provide a means to understand and rationalize fluctuations in the latent heats, and hence provide insight into the size dependence of cluster melting.

Many of the aluminum clusters that have enhanced solid cohesive energies are located near electronic shell closings, so the corresponding latent heat maxima are also induced by the same favorable electron shell structure. This differs from the related case of sodium clusters, where purely geometrical arguments explain the size dependence of the latent heats.<sup>8,11,24,25</sup> We have previously shown<sup>18</sup> for sodium clusters with around 147 atoms that the solid cohesive energies show a marked maximum at the geometrical shell closing but not at the nearby electronic shell closing. Therefore, the correlation between latent heats and solid cohesive energies holds also for sodium clusters with around 147 atoms, although it has a different (purely structural) origin.

In this section we will try to rationalize some of the other experimental observations on the melting of aluminum clusters by analyzing just the outcome of static (0 K) calculations, although explicit simulations of the melting process will be needed to confirm the proposed interpretations. For example, the experimental results obtain two well-separated heat capacity peaks for anions with 45, 46, and 65 atoms. Precisely for those sizes, theory predicts that ordered (sf or fcc) and disordered structural families are nearly degenerate in energy. It is therefore tempting to interpret the premelting peaks as signatures of solid-solid transitions between very different structures.

The melting temperature is known to exhibit a smoother size dependence than other melting properties because of the correlation between latent heats and melting entropies which tends to damp the size variations in the melting temperatures through the Clausius–Clapeyron relation. The most prominent features in the melting temperatures are the maxima that occur at around 35–37, 45–47, and 64–68 atoms (see Fig. 4). These maxima are correlated with electronic shell closings at around  $n=36$ , 46, and 66 (see above). The spherical electronic shell closings at 46 and 66 atoms stabilize nearly spherical disordered geometries, which are the lowest energy structures found for  $n=66$  and  $\text{Al}_{46}^+$  and are competitive for  $\text{Al}_{46}^-$ . There are also competitive amorphous structures around  $n=36$  shell closing, although those are not spherical. The entropy change for melting of the disordered geometries is expected to be lower than for melting of the more-ordered ddf, fcc, and sf geometries, and this may account for the elevated melting temperatures near the electronic shell closings. Note that even if the disordered structure is not the lowest energy geometry, it may become the lowest free energy geometry as the temperature is raised, and then melting will occur from the disordered structure at an elevated temperature. As noted above there is evidence for solid-solid transitions near the electronic shell closings.

Figure 10 shows the relationship between the melting temperatures and the low energy geometries found in the

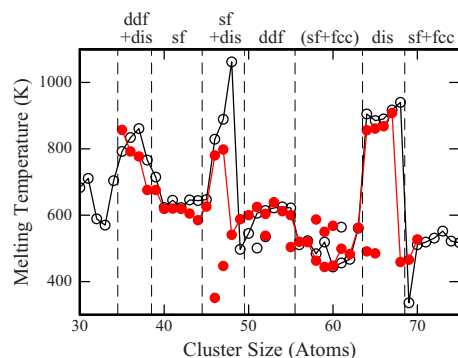


FIG. 10. Plot showing the relationship between the melting temperatures of the aluminum cluster anions and cations and the structures of the aluminum clusters as determined from the DFT calculations. The dashed lines show approximately where transitions between different structural families occur for the anions. As noted above, the transition for the cations occurs at similar sizes (usually slightly larger). The labels above the plot identify the structural families described in the text: ddf=distorted decahedral fragments, dis=disordered isomers, fcc=fcc-like fragments, and sf=fcc-like fragments with stacking faults.

calculations. The dashed lines in this figure show approximately where transitions occur between the different structural families for the anions. As noted above, the transition for the cations occurs at similar sizes (usually slightly larger). The melting temperatures generally show a fairly smooth size evolution within each structural family and much larger variations at those sizes corresponding to a structural transition. For example, the melting temperatures for clusters with 39–44 atoms, where the lowest energy geometries belong to the sf family, are around 600–700 K. For clusters with 50–55 atoms (which belong to the ddf family) the melting temperatures are all around 600 K. The drop in the melting temperature at  $n=56$  probably results from a geometry change. The melting temperature seems to be a more useful indicator of structural transitions than the latent heat. The stabilities (and latent heats) of the two competing structures are similar when the structural transition occurs, and so the difference in the melting temperature must result mainly from a difference in the entropy change for melting.

The features in the melting temperature plot for the anions are systematically shifted to slightly lower sizes than for cations (see Fig. 4). As explained above, the theoretical calculations predict that the same sequence of structural transitions occurs for both anions and cations, so the two melting temperature plots should have similar global shapes. But theory also finds that all the structural transitions for anions occur at smaller sizes than for cations, which explains the global shift seen in Fig. 4. For example, while  $\text{Al}_{68}^+$  still adopts a disordered structure,  $\text{Al}_{68}^-$  is already an ordered sf structure, so the drop in melting point occurs at  $n=68$  for anions and  $n=69$  for cations. A similar interpretation holds for the other transitions.

In the vicinity of a structural transition, there are two structural families which closely compete in energy. The contribution to the cohesive energy coming from the electron shell structure may be the key factor in deciding which structure is the global minimum energy isomer for these sizes. The cluster anion  $\text{Al}_n^-$  has one electron less than  $\text{Al}_{n+1}^+$  but two more electrons than  $\text{Al}_n^+$ , so it can be considered more

similar to  $Al_{n+1}^+$  from the electronic point of view. This may be the reason why, close to the critical transition sizes,  $Al_n^-$  prefers to adopt a structure of the same family as  $Al_{n+1}^+$ .

Up to now, we have discussed the *size* dependence of cohesive energies and melting properties for both cations and anions. It remains for us to get some physical insight into the significant *charge* dependence of melting properties, which is observed for some anions and cations with the same number of atoms. This dependence is most striking for those sizes where anion and cation share the same global minimum structure. For example, the structure of clusters with 35 atoms is the same for anions, cations, and neutrals, but the latent heat of the anion is about 0.8 eV larger than the latent heat of the cation. The melting temperature is also significantly higher for the anion. This is surprising given the previous results for sodium clusters, where purely geometrical arguments dictate the melting parameters. It seems that the electron shell structure can be significantly different in the solid and liquid phases of aluminum clusters.

Even if the global minimum structure is the same, there might still be some subtle structural differences: The average bond length or the distribution of bond lengths, for example, can depend on the cluster charge. To explore this idea further, we have calculated the average bond length for each size and found that it is always shorter (i.e., the bond strength is higher) at the electron shell closings. For example, for  $n=35$  the anion is more compact than for both neutral and cation; for  $n=36$  the neutral has the shortest average bond length, while for  $n=37$  it is the cation that is more compact. But the differences are small, of the order of only 0.1%, which is hardly significant. In addition, we have evaluated the normal mode vibrational frequencies by diagonalizing the force constant matrix. The geometric mean of the vibrational frequencies, which enters the quasiharmonic expression for entropy, is always higher (i.e., the bonds are stiffer) at the electron shell closings, but once more the differences are small, less than 1%. We have also evaluated the difference between the vertical and adiabatic ionization energies, which is on the order of 0.1 eV for all sizes. This difference is an approximate measure of the energy involved in structural relaxation upon changing just the number of electrons, and it is clearly much smaller than the typical differences between latent heats of the anions and cations (see Fig. 5). We conclude that the large differences in melting properties that occur for cluster sizes sharing the same structure must have a purely energetic origin coming from the stabilization due to electronic shell closings.

In the following, we devise an approximate model which allows a qualitative interpretation of the charge dependence of the melting properties, employing only the results from static calculations. The experiments demonstrate that the dissociation energies of liquid clusters change much more smoothly with cluster size than the dissociation energies of the solid clusters, and so we expect that the ionization energies and electron affinities of liquid clusters will also have a much smoother size dependence than the corresponding values for the solid clusters. Let us approximate the ionization energies and electron affinities in the liquidlike phase by the smooth dashed curves shown in Fig. 9, which are obtained

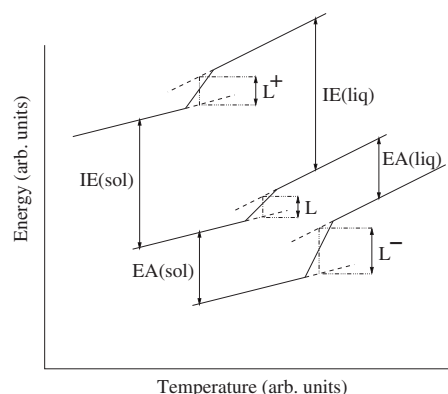


FIG. 11. A schematic diagram showing the relationship between the caloric curves of cluster cations (top curve), neutrals (middle curve), and anions (bottom curve) for a fixed cluster size. Different melting temperatures and latent heats are shown for each charge state. Solid lines show the solid (low temperature) and liquid (high temperature) branches of the caloric curves and dashed lines are employed to represent the extensions of the solid and liquid branches of the caloric curves into the melting region. The latent heats are defined as the energy differences between the solid and liquid branch extensions evaluated at the middle point of the transition region. The slope is always larger in the liquid branches because the liquid has a larger heat capacity than the solid. We only show the temperature interval closely bracketing the melting temperatures, and hence we do not show explicitly that the slope of the caloric curves goes to zero at very low temperatures.

by fitting the solidlike values to a classical charged sphere model. Of course this is a rough approximation (for example, the liquid clusters will have an expanded volume as compared to the solid ones, which will cause some systematic error), but we will show that it is accurate enough for our purpose.

Figure 11 shows a schematic plot of the caloric curves of anions, neutrals, and cations for a fixed number of atoms. From that figure one can directly obtain the following approximate relations:

$$L - L^+ = IE(\text{sol}) - IE(\text{liq}) \quad (13)$$

and

$$L^- - L^+ = [IE(\text{sol}) + EA(\text{sol})] - [IE(\text{liq}) + EA(\text{liq})], \quad (14)$$

where  $L^+$ ,  $L$ , and  $L^-$  are the latent heats of the cation, neutral, and anion, respectively. So it is the melting-induced change in the sum of ionization energy and electron affinity which drives the latent heat differences between cations and anions. These relations, together with our approximation for the liquid ionization energies and electron affinities, can be used to predict the latent heats of neutral ( $L - L^+$ ) and anionic ( $L^- - L^+$ ) clusters taking as a reference the cationic values.

Table I shows a few examples that demonstrate the general validity of the proposed model. The anion values can be directly compared to the experimental ( $L^- - L^+$ ) differences, while the neutral values are only a theoretical prediction. The model succeeds in reproducing the experimental variations in the latent heats with cluster charge for all sizes, except those where theory was not able to locate the correct global minimum (sizes  $n=37$  and  $n=59$  are provided in Table I as examples). For  $n=35$ , for example, *both* the ionization energy and electron affinity are significantly higher than the average. According to our simple model, the latent heat should be

TABLE I. The difference between the measured latent heats of the anions and cations,  $(L^- - L^+)_{\text{expt}}$  for representative cluster sizes is compared to the values obtained from the calculations,  $(L^- - L^+)_{\text{th}}$ .  $(L^- - L^+)_{\text{th}}$  is the theoretical prediction for the difference between the latent heats of neutrals and cations.

Number of atoms	$(L^- - L^+)_{\text{expt}}$ (eV)	$(L^- - L^+)_{\text{th}}$ (eV)	$(L^- - L^+)_{\text{th}}$ (eV)
35	+0.77	+0.65	+0.22
36	+0.02	-0.05	+0.39
37	-0.08	-0.51	-0.47
39	-0.60	-0.56	-0.43
40	+0.11	+0.19	+0.10
43	-0.29	-0.30	-0.37
44	-0.37	-0.40	-0.12
51	+0.16	+0.13	-0.08
52	-0.01	-0.06	+0.18
59	+0.87	+0.25	-0.03
64	+0.19	+0.16	+0.16
65	+0.07	+0.16	+0.07
66	+0.05	-0.05	+0.25
67	-0.07	-0.15	-0.19
69	+0.42	+0.35	+0.13

significantly larger for the anion, than for the cation. For  $n = 36$ , the ionization energy is larger and the electron affinity is lower than the average trend; both contributions cancel almost perfectly so the latent heats of the anion and the cation are very similar. However, the latent heat of the neutral is predicted to be significantly larger than that for any of the charged clusters. Exactly the same trend is observed for  $n = 66$ . For clusters with 43 and 44 atoms, the cation clusters have larger latent heats than the anions due to a very low ionization energy for  $n=43$  and to a very low electron affinity for  $n=44$ , compared to the average liquid trend. All these theoretical predictions are closely followed by the experimental observations. Other features can be explained in similar terms.

It is gratifying that a simple physical model can rationalize the apparently complex dependence of the measured latent heats on the charge state of the cluster, even when the global minimum structure is the same. We think that the nice agreement convincingly confirms that some electronic properties such as the ionization energies and electron affinities can be very different in the solid and liquid states of the cluster. A careful analysis of static calculations can be useful in interpreting melting properties. The results also demonstrate the utility of theoretically determining the structure of *neutral* clusters, as these are needed as intermediates to connect the behavior of cation and anion clusters.

## VII. CONCLUSIONS

Melting temperatures, latent heats, and cohesive energies measured for aluminum cluster anions show the same global trends as observed for the corresponding cations, but substantial differences emerge for some cluster sizes.

The lowest energy geometries found in the calculations of aluminum cluster anions are similar to those obtained for the corresponding cations. Anions, cations, and neutral clusters show the same structural families and same sequence of

structural changes occurs with increasing cluster size. For some clusters (for example,  $n=37$  and 57) the agreement with the measured cohesive energy is poor, and it is likely that the ground state geometry has not been located.

The measured cohesive energies of liquid aluminum cluster anions and cations change smoothly with cluster size and so the size-dependent variations in the cohesive energies of the solid clusters result almost entirely from the latent heats. Thus differences in the latent heats can be understood using static calculations of the cohesive energies. As in the case of the cations, we find that the cohesive energies (and hence the latent heats) are influenced by both geometric and electronic shell closings.

At the transition points between structural families, the different structures have similar cohesive energies and hence similar latent heats, and so the latent heats (and cohesive energies) do not provide a signature of the structural transition. On the other hand, abrupt changes in the melting temperatures occur at the transition points between different structural families.

Prominent maxima in the melting temperatures are correlated with electronic shell closings at 36, 46, and 66 atoms. Disordered geometries are stabilized near the electronic shell closings. For some cluster sizes the disordered geometry becomes the ground state, for others it may become the lowest free energy structure as the temperature is raised. Melting from the disordered geometry is expected to occur at an elevated temperature because of the diminished entropy change.

The plot of the melting temperature against cluster size for aluminum cluster anions is systematically shifted to smaller cluster sizes than the cations. Calculations show that the structural transitions that occur with increasing cluster size always occur for the anions at smaller cluster sizes than for the corresponding cations.

We describe an approximate model that can account for the charge dependence of the latent heats using the ionization energies and electron affinities of the solid and liquid clusters. The results show that the electron affinities and ionization energies can be very different in the solid and liquid states of the cluster, indicating that the electronic structure can change substantially when the cluster melts.

## ACKNOWLEDGMENTS

We gratefully acknowledge the support of the National Science Foundation, Junta de Castilla y León, the Spanish MEC, and the European Regional Development Fund (Project Nos. FIS2008-02490/FIS and GR120).

<sup>1</sup>M. Schmidt, R. Kusche, W. Kronmüller, B. von Issendorff, and H. Haberland, *Phys. Rev. Lett.* **79**, 99 (1997).

<sup>2</sup>M. Schmidt, R. Kusche, B. von Issendorff, and H. Haberland, *Nature (London)* **393**, 238 (1998).

<sup>3</sup>R. Kusche, Th. Hippler, M. Schmidt, B. von Issendorff, and H. Haberland, *Eur. Phys. J. D* **9**, 1 (1999).

<sup>4</sup>M. Schmidt, R. Kusche, T. Hippler, J. Donges, W. Kronmüller, B. von Issendorff, and H. Haberland, *Phys. Rev. Lett.* **86**, 1191 (2001).

<sup>5</sup>M. Schmidt, T. Hippler, J. Donges, W. Kronmüller, B. von Issendorff, H. Haberland, and P. Labastie, *Phys. Rev. Lett.* **87**, 203402 (2001).

<sup>6</sup>M. Schmidt and H. Haberland, *C. R. Phys.* **3**, 327 (2002).

<sup>7</sup>M. Schmidt, J. Donges, T. Hippler, and H. Haberland, *Phys. Rev. Lett.*

- 90**, 103401 (2003).
- <sup>8</sup> H. Haberland, T. Hippler, J. Donges, O. Kostko, M. Schmidt, and B. von Issendorff, *Phys. Rev. Lett.* **94**, 035701 (2005).
- <sup>9</sup> C. Hock, S. Strassburg, H. Haberland, B. von Issendorff, A. Aguado, and M. Schmidt, *Phys. Rev. Lett.* **101**, 023401 (2008).
- <sup>10</sup> F. Chirof, P. Feiden, S. Zamith, P. Labastie, and J. M. L'Hermite, *J. Chem. Phys.* **129**, 164514 (2008).
- <sup>11</sup> C. Hock, C. Bartels, S. Strassburg, M. Schmidt, H. Haberland, B. von Issendorff, and A. Aguado, *Phys. Rev. Lett.* **102**, 043401 (2009).
- <sup>12</sup> G. A. Breaux, C. M. Neal, B. Cao, and M. F. Jarrold, *Phys. Rev. Lett.* **94**, 173401 (2005).
- <sup>13</sup> C. M. Neal, A. K. Starace, and M. F. Jarrold, *Phys. Rev. B* **76**, 054113 (2007).
- <sup>14</sup> C. M. Neal, A. K. Starace, and M. F. Jarrold, *J. Am. Soc. Mass Spectrom.* **18**, 74 (2007).
- <sup>15</sup> B. Cao, C. M. Neal, A. K. Starace, Y. N. Ovchinnikov, V. Z. Kresin, and M. F. Jarrold, *J. Supercond. Novel Magn.* **21**, 163 (2008).
- <sup>16</sup> M. F. Jarrold, B. Cao, A. K. Starace, C. M. Neal, and O. H. Judd, *J. Chem. Phys.* **129**, 014503 (2008).
- <sup>17</sup> B. Cao, A. K. Starace, C. M. Neal, M. F. Jarrold, S. Núñez, J. M. López, and A. Aguado, *J. Chem. Phys.* **129**, 124709 (2008).
- <sup>18</sup> A. K. Starace, C. M. Neal, B. Cao, M. F. Jarrold, A. Aguado, and J. M. López, *J. Chem. Phys.* **129**, 144702 (2008).
- <sup>19</sup> W. A. de Heer, *Rev. Mod. Phys.* **65**, 611 (1993).
- <sup>20</sup> M. Brack, *Rev. Mod. Phys.* **65**, 677 (1993).
- <sup>21</sup> W. D. Knight, K. Clemenger, W. A. de Heer, W. A. Saunders, M. Y. Chou, and M. L. Cohen, *Phys. Rev. Lett.* **52**, 2141 (1984).
- <sup>22</sup> C. Brechignac, P. Cahuzac, J. Leygnier, and J. Weiner, *J. Chem. Phys.* **90**, 1492 (1989).
- <sup>23</sup> K. Clemenger, *Phys. Rev. B* **32**, 1359 (1985).
- <sup>24</sup> A. Aguado and J. M. López, *Phys. Rev. Lett.* **94**, 233401 (2005).
- <sup>25</sup> A. Aguado, *J. Phys. Chem. B* **109**, 13043 (2005).
- <sup>26</sup> A. Aguado and J. M. López, *Phys. Rev. B* **74**, 115403 (2006).
- <sup>27</sup> S. M. Ghazi, M. Lee, and D. G. Kanhere, *J. Chem. Phys.* **128**, 104701 (2008).
- <sup>28</sup> C. M. Neal, G. A. Breaux, B. Cao, A. K. Starace, and M. F. Jarrold, *Rev. Sci. Instrum.* **78**, 075108 (2007).
- <sup>29</sup> J. Bohr, *Int. J. Quantum Chem.* **84**, 249 (2001).
- <sup>30</sup> R. S. Berry, J. Jellinek, and G. Natanson, *Phys. Rev. A* **30**, 919 (1984).
- <sup>31</sup> T. L. Beck, J. Jellinek, and R. S. Berry, *J. Chem. Phys.* **87**, 545 (1987).
- <sup>32</sup> J. P. Rose and R. S. Berry, *J. Chem. Phys.* **98**, 3246 (1993).
- <sup>33</sup> B. Vekhter and R. S. Berry, *J. Chem. Phys.* **106**, 6456 (1997).
- <sup>34</sup> O. K. Rice and H. C. Ramsperger, *J. Am. Chem. Soc.* **50**, 617 (1928).
- <sup>35</sup> W. Kohn and L. J. Sham, *Phys. Rev.* **140**, A1133 (1965).
- <sup>36</sup> J. M. Soler, E. Artacho, J. D. Gale, A. García, J. Junquera, P. Ordejón, and D. Sánchez-Portal, *J. Phys.: Condens. Matter* **14**, 2745 (2002).
- <sup>37</sup> J. P. Perdew, K. Burke, and M. Ernzerhof, *Phys. Rev. Lett.* **77**, 3865 (1996); **78**, 1396 (1997).
- <sup>38</sup> A. Aguado and J. M. López, *J. Phys. Chem. B* **110**, 14020 (2006).
- <sup>39</sup> A. Aguado and J. M. López, *J. Chem. Phys.* **130**, 064704 (2009).
- <sup>40</sup> D. J. Henry, A. Varano, and I. Yarovsky, *J. Phys. Chem. A* **112**, 9835 (2008).
- <sup>41</sup> "Nanometric Properties of Matter" Research Group, <http://metodos.fam.cie.uva.es/~GIR>.
- <sup>42</sup> M. Lei, K. Maijer, B. von Issendorff, and A. Aguado (unpublished).
- <sup>43</sup> K. E. Schriver, J. L. Persson, E. C. Honea, and R. L. Whetten, *Phys. Rev. Lett.* **64**, 2539 (1990).